NASA TECHNICAL MEMORANDUM

NASA TM X-67973

NASA TM X-67973

A TURBOJET SIMULATOR FOR MACH NUMBERS UP TO 2.0

by Fred W. Steffen, Edward A. Satmary,
Michael R. Vanco, and Stanley M. Nosek
Lewis Research Center
Cleveland, Ohio

TECHNICAL PAPER proposed for presentation at
Sixteenth Annual International Gas Turbine Conference and Products Show - sponsored by the American Society of Mechanical Engineers
San Francisco, California, March 23-30, 1972

A TURBOJET SIMULATOR FOR MACH NUMBERS UP TO 2.0

by Fred W. Steffen, Edward A. Satmary,
Michael R. Vanco, and Stanley M. Nosek

National Aeronautics and Space Administration
Lewis Research Center
Cleveland, Ohio

E-6690

ABSTRACT

A turbojet simulator has been designed and fabricated for use in wind tunnel models. The simulator contains a six-stage, axial-flow compressor powered by a three-stage, axial-flow turbine. High pressure heated air was used to drive the turbine. At design conditions, compressor axial flow, turbine exit flow, and a third supplementary flow all entered the exhaust nozzle at equal values of pressure and temperature. Overall aerodynamic design, compressor operating conditions, automatic controls, turbine aerodynamic design, instrumentation, and calibration procedure is presented. Performance of the device when used to simulate a J-85 turbojet engine at transonic speeds is reported. The installed nozzle performance obtained with the simulator is also discussed and compared with flight data.

INTRODUCTION

For some wind tunnel research programs, it is necessary to simultaneously simulate the inlet flow and exhaust flow of a jet propelled aircraft. In recent years, for example, the propulsion interference drag of subsonic fan-jet aircraft has been studied with the aid of fan-jet engine simulators. References 1 and 2 report the use of this technique. Typically, these simulators have a fan driven by an air turbine. The fan

and turbine are mounted on a common shaft. The turbine drive air is obtained from an external supply at moderate temperatures. Both the fan and the turbine drive air exhaust from the simulator.

Nozzle research programs at the Lewis Research Center dictated the need for a modern high-pressure ratio turbojet engine simulator which could be operated in the 8- by 6-Foot Supersonic Wind Tunnel at transonic and supersonic speeds up to Mach 2.0. This simulator would differ from existing fan-jet simulators in that high engine and nozzle pressure ratios would be necessary and that all flows would exit through a common nozzle. The initial programs required the simulation of two particular propulsion parameters; inlet mass flow ratio and exhaust nozzle pressure ratio. An engine simulator to perform this task, with the air supplies available at the 8- by 6-Foot Supersonic Wind Tunnel, was therefore designed and fabricated.

The primary purpose of this paper is to present the aerodynamic and mechanical design features of the simulator as well as the simulator's performance during its initial application. A secondary purpose is to present some installed nozzle performance results and compare them with flight results.

The simulator was first used in conjunction with the nozzle flight test program currently in progress at the Lewis Research Center. The flight test program uses a General Electric J-85-13 turbojet engine mounted beneath the wing of an F-106B aircraft to obtain installed nozzle performance data at Mach numbers between 0.6 and 1.3 as described in reference 3. To provide a comparison of wind tunnel and flight test data, the simulator was mounted beneath the wing of a 0.22 scale half-plane

model of an F-106B in the 8- by 6-Foot Supersonic Wind Tunnel.

Tests were made at Mach numbers from 0.6 to 1.27. Inlet mass-flow ratio and nozzle pressure ratio were varied over a sufficient range at each Mach number to include the values of these parameters which had been obtained with the J-85-13 engine during full-scale flight tests.

SYMBOLS

D	drag, lb
F_g	gross nozzle thrust, lb
F_{IP}	ideal gross thrust of the primary nozzle
F_s	force measured by strain link, lb
g	gravitational constant, 32.17 ft/sec^2
h	enthalpy, Btu/lb
$\Delta h'$	stage specific work output, Btu/lb
J	mechanical equivalent of heat, 778 ft-lb/Btu
M_0	free stream Mach number
m	mass flow rate, slugs/sec
N	rotational speed, rpm
P	total pressure, lb/in.^{2} abs
p	static pressure, lb/in.^{2} abs
T	total temperature, $^\circ$R
U	blade speed at the mean diameter, ft/sec
W	weight flow rate, lb/sec
δ	P/14.7
θ	T/518.6
λ	stage speed-work parameter, $U^2/gJ\,\Delta h'$
τ	T_s/T_p
ω	W_s/W_p

Subscripts:

b	base
bm	bellmouth
mu	make-up
p	primary
s	secondary
T	turbine
0	free stream
2	compressor inlet
3	compressor exit
3'	compressor flow passage exit
4	turbine inlet
5	turbine exit
7	nozzle inlet
8	nozzle throat

OVERALL AERODYNAMIC DESIGN

The aerodynamic design of the turbojet simulator is based on the use of the six-stage axial compressor from the Allison T63 turboshaft engine. Its compact design and its relatively high mass flow and pressure ratio characteristics, plus the fact that it was a developed compressor in production, were the factors that led to its selection as the critical component on which to base the simulator design. The design evolved is shown in the isometric drawing of the simulator in figure 1 and schematically in figure 2.

The inlet air is compressed by the compressor and supplied to the nozzle through an annulus around the turbine. Since the flow is not re-

quired to leave the compressor axially in the T-63 engine, it was necessary to place a stage of straightening vanes behind the last compressor stage. The outside diameter of the annulus was kept at the same diameter as the tip of the compressor, 4.3 inches. The inside diameter was increased from 3.1 inches at the hub of the compressor to 3.5 inches at the rear of the mid-frame struts and then maintained constant around the turbine.

The turbine to drive the compressor is a three-stage turbine with a constant tip diameter. It is powered by an external supply of 450 psia air that could be heated to 700° F. The air was supplied to an annular chamber around the engine and then through five of the six struts of the mid frame to an inner chamber feeding the turbine. (The top strut, which was aligned with the turbine air supply line, was blocked to obtain better distribution of the flow.) The air expands through the turbine and discharges into an annulus and then is combined with the stream from the compressor.

To obtain a desired ratio of nozzle throat area to engine inlet area and maintain proper nozzle pressure ratios, makeup air is supplied to fill the nozzle. The makeup air is supplied to an annular chamber from which it is fed to the nozzle through a 1/8-inch annulus concentric with the annulus from the compressor.

To improve the uniformity of the flow, the three concentric streams are passed through a "daisy" mixer, shown in figure 3, before entering the nozzle. The mixer was designed to rearrange the flow into eight radial lobes while maintaining a constant flow area in each of the three flow passages.

Finally, secondary air was supplied concentric with the outside of the nozzle to simulate nozzle cooling flow.

TURBINE AERODYNAMIC DESIGN

The turbine has a constant tip diameter of 3.2 inches. The inlet hub diameter was selected at 2.7 inches to give a reasonable blade height. The exit hub diameter was governed by the bearing size and was selected at 2.0 inches. The turbine flow path is shown in figure 4.

The turbine was designed for a compressor speed of 63 000 rpm, compressor power of 402 H.P. (284 Btu/sec), and exit total pressure of 60 psia. The exit pressure was specified because it was important to match the compressor and turbine exit pressures to obtain good exhaust nozzle inlet profiles.

The air supply to drive the turbine was capable of pressures up to 450 psia and temperatures up to 750° F. Considering losses in the ducts, the design values chosen were turbine inlet temperature of 700° F and pressure of 358 psia. The design value of turbine overall total efficiency was 0.785. To obtain this efficiency, it was specified that the turbine have a stage speed-work parameter, λ, of 0.78 at the average mean diameter. Because of the small size and the high blade row reaction which results in higher clearance losses, conservative values of total efficiency for the first and second stages of 0.73 and 0.77 were selected. The geometry and the number of blades for the resulting three stage turbine are given in table I. The axial spacing between the blade rows is 0.0625" and rotor tip clearance is 0.010".

The blading used in the turbine of reference 4, which was based on symmetrical velocity diagrams, was used for the turbojet simulator blad-

ing. The first stage stator blading of reference 4 was used for the first stage stator and third stage rotor blading of the simulator turbine while the interstage stator blading of reference 4 was used for all other blading in the simulator turbine. The stagger angles of these blades were adjusted to obtain the proper throat areas and exit angles. To simplify fabrication, it was specified that all blades have constant sections with no twist. The velocity levels in this design were low enough so that the resulting incidence losses would be small. The turbine stators and rotors are shown in figure 5.

An analytical off-design performance map was determined by using the method of reference 5. The performance map is shown in figure 6. This map, along with the compressor map, was used to arrive at operating conditions for the simulator.

Mechanical Design

The major components of the simulator are shown in figure 7. The compressor is a modified T-63-A-5A model 250-C19 six-stage axial flow unit. Two modifications were made by Allison under contract to NASA. The first was the removal of the fifth stage bleed plenum to provide a smaller compressor envelope. The second was the structural modification of the fifth and sixth-stage compressor wheels for increased burst speed. The new burst speed was calculated to be 75 600 rpm. The individual compressor rotors were held together as one unit by means of a central tie bolt which was also used as a means of rigidly coupling the compressor and turbine drive shaft.

The turbine rotors had integral blades and hubs, and were machined by electric discharge techniques from 17-4-P11 steel. This is a precipi-

tating hardening steel widely used for its strength at elevated temperatures, for its machinability, and for its dimensional stability. The rotors were keyed to the turbine drive shaft. A labyrinth seal is incorporated into the rotor disc to minimize interstage flow.

The stator airfoils and hubs were also of one-piece construction. However, each stator had a shroud furnace brazed to the airfoil tips. When the individual stator units were stacked together, the shrouds formed the outer wall of the turbine flow annulus and the inner wall of the compressor flow annulus. The I.D. of the stator hubs was flame sprayed with a coating of an abraidable material (an 0.025-in. thick nickel graphite mixture). This surface was machined to give a close fit with the labyrinths on the rotors.

Electric discharge machining and furnace brazing were also used in the fabrication of the mid-bearing and rear-bearing housings. The thick struts in the main bearing housing carried the turbine drive air from an outer annulus to an inner annulus. These struts also carried oil and instrumentation lines. The thin struts in the rear bearing housing served as lubrication system oil and vent lines. The three bearings each operated under different conditions. A close tolerance bearing (furnished by Allison as a part of the compressor) was used as the front bearing since it operated at ambient temperature and carried very little thrust load. The middle bearing carried the largest part of the thrust load and was located in the immediate vicinity of the turbine drive air. The bearing (ABEC-7) had a split inner race, and was fabricated from high-temperature materials. The rear bearing, although not required to carry thrust loads, was also a high temperature precision bearing.

Carbon shaft seals were used to contain the lubricating oil for the mid bearing. These contained double rows of segmented, spring-loaded carbon elements. The two rows were separated by a central chamber which, when pressurized with air, allowed very little leakage of oil. A carbon face seal is used in the rear bearing housing as the barrier between the turbine air and the rear bearing lube oil.

STRESS AND VIBRATION ANALYSIS

The airfoils for both the compressor and turbine were analyzed for steady state and dynamic stresses. They were found to be quite safe up to 63 000 rpm.

A dynamic analysis was made for the complete rotating unit to define critical speeds. The shaft was considered to be rigidly supported by the two rear bearings but only softly supported by the front bearing. Several critical speeds were calculated and observed during tests of the simulator. At these speeds, the instrumentation recorded a small increase in G loading and whip but no serious problems arose.

Simulator Air Supply and Control Systems

A 450 psi continuous flow air supply system was used to drive the simulator. This system and its controls are shown in figure 8. The air was routed both through and around a gas fired heat exchanger which was maintained at a constant temperature of about 700^{o} F. The heated and unheated flows were then combined in mixing valves to rapidly achieve the desired turbine and makeup air temperatures.

Rotational speed, turbine inlet temperature, makeup air pressure, and makeup air temperature were each controlled by a separate closed-loop control system. The rotational speed control compared measured speed to

set speed and sent an error signal to a throttle valve in the turbine air line. The rotational speed control prevented significant speed variations from occurring during compressor stalls, as well as during routine changes of other variables.

The turbine inlet temperature control compared measured turbine inlet temperature to set turbine inlet temperature and sent an error signal to the turbine air mixing valve. Thus, the desired value of turbine inlet temperature (as determined by the desire to match compressor and turbine outlet temperature) could be maintained regardless of turbine air flow rate.

Pressure and temperature controllers in the makeup air line also sent error signals to the makeup air throttle valve and the makeup air mixing valve, respectively. Thus, makeup air pressure (as determined by desired nozzle pressure ratio) and makeup air temperature (as determined by the desire to match the temperature of all flows entering the nozzle) could be maintained regardless of makeup flow rate.

INSTRUMENTATION

The instrumentation required for the nozzle performance program including the calibration phase, is shown in figure 9. Turbine, makeup, and secondary airflow rates were obtained with calibrated, sharp-edged orifices. Much of the instrumentation shown with the calibration nozzle was used only for initial flow calibrations and had to be minimized during force tests to reduce the friction caused by the tubing and wire leadouts. Also shown is the instrumentation necessary to determine the aerodynamic performance of the simulator.

Although not shown in figure 9, instrumentation for monitoring the

mechanical condition of the simulator and providing shut-down inputs to the control system was also installed. Included in this category were two accelerometers, two whip pickups, thermocouples for measuring oil temperature, and pressure transducers and gages for measuring oil pressure to the bearings and air pressure to the middle bearing seals.

Test Procedure

As mentioned in the Introduction, the simulator was mounted beneath the wing of a 0.22 scale half-plane model of an F-106B in the 8- by 6-Foot Supersonic Wind Tunnel. The installation of this model in the tunnel is shown in figure 10. The fuselage was mounted on a reflection plane which was located five inches away from the perforated wall of the tunnel. This arrangement allowed the tunnel wall boundary layer to pass beneath the reflection plane. The entire installation resulted in a tunnel blockage of about 2.9%. Although angle of attack could be varied from 0 through 8 degrees, an angle of attack of 3° was used for all of the data presented in this paper.

To obtain installed nozzle performance data, five steps were required.

Step I. - The calibration configuration consisting of the bellmouth inlet and the calibration nozzle, figure 11(a), was statically tested. The calibration nozzle was a long radius ASME nozzle with a shielded blunt base area. For this step, the configuration had full nozzle inlet and base instrumentation. The purpose of this step was to confirm the estimated calibration nozzle flow coefficient of 0.9930 and check the turbine and make-up air flow measuring systems. This was done by dividing the sum of the bellmouth flow, turbine drive flow, and makeup flow by an ideal nozzle flow (based on nozzle inlet pressure, temperature, and area)

to obtain a nozzle flow coefficient. For choked nozzle conditions, this method gave a mean flow coefficient of 0.9933 with a standard deviation of 0.017, thus establishing the credibility of the individual flow measurements and confirming the estimated nozzle flow coefficient.

Step II. - The calibration configuration consisting of the normal shock inlet and the calibration nozzle, figure 11(b), was tested next at Mach numbers of 0.6, 0.9, and 1.27 with full nozzle inlet and base instrumentation. Since the leads from the full nozzle instrumentation used in Steps I and II interfered with the nacelle thrust balance reading, the data obtained in Step II, as well as in Step I, was thus used to select two nozzle inlet pressure probes, two nozzle inlet thermocouples, and two base pressure taps which gave the closest to the average values of these readings. All other nozzle instrumentation leads were then removed so that thrust could be measured in succeeding tests.

Step III. - The static calibration configuration, figure 11(a) was again tested but with the reduced instrumentation. The purpose of this test was to establish the credibility of the force measuring system and confirm the estimated calibration nozzle thrust characteristics. To do this, the measured thrust, corrected for bellmouth forces, was compared to the nozzle thrust based on nozzle inlet pressure and an estimated value of stream thrust parameter, $\frac{m_8 V_8 + p_8 A_8}{P_8 A_8}$, of 1.259. The mean measured value of stream thrust parameter was 1.264 with a standard deviation of 0.031, thus establishing the credibility of the force measuring system and confirming the estimated value of the stream thrust parameter.

Step IV. - The calibration configuration consisting of the normal shock inlet and calibration nozzle with reduced instrumentation, fig-

ure 11(b), was then tested over a range of Mach numbers from 0.6 to 1.27. The main purpose of these tests was to establish the tare drag of the nacelle as a function of free-stream Mach number and inlet mass flow ratio. The tare drag was defined to include the free-stream momentum drag, additive drag, and all nacelle and strut drag forward of the nozzle attachment station. The tare drag was obtained by subtracting the sum of the thrust link strain gage reading, the measured base pressure drag, and the estimated skin friction drag acting aft of the nozzle attachment station from the jet thrust of the calibration nozzle (based on nozzle inlet pressure and the confirmed value of stream thrust parameter).

These tests were also used to determine the flow through the normal shock inlet as a function of p_2, P_2, and T_2. The inlet flow was obtained by subtracting the measured turbine and makeup flows from the nozzle flow (again based on nozzle inlet pressure and temperature and a confirmed nozzle flow coefficient).

Step V. - Finally, the research nozzle performance tests with the configurations shown in figure 12 were made. These nozzles were the variable flap ejector nozzle (VFE nozzle) and the auxiliary inlet ejector nozzle (AIE nozzle). In these tests, nozzle weight flow was obtained by summing the calibrated normal shock inlet flow and the turbine and makeup flows. Nozzle thrust minus drag was determined by adding the nacelle tare drag to the force measured by the thrust link strain gage.

The overall dimensions of the nacelle with various nozzles and inlets installed are shown in figure 13. The VFE and AIE nozzles used the same primary nozzle. The actuating mechanism blockage of the J-85-13

primary nozzle was simulated by a ring containing twelve slots. Secondary air was diverted through these slots to simulate primary nozzle cooling air.

For both the calibration and performance tests, the two parameters to be simulated, namely inlet mass flow ratio and nozzle pressure ratio, were varied over a small range at each Mach number. Inlet mass flow ratio and nozzle pressure ratio were varied independently by simultaneously varying compressor speed and makeup flow rate. Visual displays of p_2/P_2 and P_7 were used to set the simulator operating conditions.

DISCUSSION OF RESULTS

J85-13 Simulator

As stated in the instrumentation section, the initial nozzle performance test program required the simulation of the inlet mass flow ratios and exhaust nozzle pressure ratios which had been achieved in flight with a J85-13 engine at minimum reheat power setting. The range of nozzle pressure ratios and inlet mass flow ratios achieved with both the turbojet simulator when fitted with a scaled minimum reheat exhaust nozzle and the J85-13 in flight tests are shown in figure 14. The actual nozzle pressure ratios for the J85-13 at minimum reheat power setting fall between the values shown for military and maximum reheat power settings. The variation of inlet mass flow ratio with corrected secondary weight flow ratio for the J85-13 occurs because the ejector secondary flow was obtained from the inlet in flight. In the simulator, secondary weight flow was obtained from an external source and usually set for $\omega\sqrt{\tau} = 0.04$. The data in figure 14 thus show that the simulator provided the desired range of inlet mass flow ratios and nozzle mass flow ratios.

In addition, the simulator was required to provide uniform pressure and temperature profiles to the exhaust nozzle. The nozzle inlet profiles with makeup air both on and off are shown in figure 15. The profiles are presented in terms of local to average ratios. With makeup air either on or off, the measure value of P/P_7 varied from about 0.98 to 1.02 and the measured value of T/T_7 varied from about 0.96 to 1.12. These profiles were considered to be satisfactory. The highest value of T/T_7 occurred toward the centerbody. Note that $T_5/T_7 = 0.95$ and $T_3'/T_7 = 1.21$. It thus appears that although the daisy mixer may have rearranged the annular flows into radial lobes, little mixing had occurred by the time the flow had reached Station 7. This further suggests that the pressures of the compressor and turbine exit flows were well matched before entering the daisy mixer. The pressure loss caused by the daisy mixer was not fully determined since P_5 was not measured. However, P_3/P_7 was found to vary from 1.10 to 1.15. All of the tests were run with turbine inlet temperatures between 500° and 550° F. It appears that an increase in this temperature would have resulted in a more uniform nozzle inlet temperature profile.

Compressor Operation

A compressor operating map for the T-63 axial flow compressor without the flow straightening vanes is shown in figure 16. Shown in the map is a typical operating line for the simulator with no makeup air. With the specific turbine design used in the simulator and the turbine inlet conditions required for good nozzle inlet profiles, the location of this line relative to the stall line was determined by the effective area of the choked simulator exhaust nozzle. The geometric throat area of the

nozzles used in these tests was 6.3 in.^{2}. With the addition of makeup air, the compressor operated in the shaded region between the no makeup air operating line and the compressor stall line. In this way, independent variation of inlet mass flow (compressor flow) and nozzle pressure ratio (related to compressor pressure ratio) was obtained. Makeup air weight flow was varied from 0 to 0.7 lbs/sec, makeup inlet air pressure was varied from 36 to 70 psia, and makeup air inlet temperature was varied from 50° to 115° F.

Turbine Operation

Re-presented in figure 17 is the analytical turbine map. Superimposed are the measured values of $\Delta h_T/\theta_4$ and $\frac{\omega_4 N}{60\delta_4}$. The total pressure ratio across the turbine was not measured. The fact that the data fell above the choke line indicates that the turbine operated more efficiently than was assumed during the turbine design phase.

Turbine weight flows varied from 1.70 lbs/sec to 2.25 lbs/sec, turbine inlet pressure varied from 180 to 236 psia, and turbine inlet temperature varied from 500° to 550° F.

Installed Nozzle Performance

A brief summary of the installed nozzle performance obtained during these tests is shown in figure 18. Data from flight and 22% scale model tests with the turbojet simulator are compared. The flight data are from references 6 and 7. Figure 18(a) shows data for the VFE nozzle and figure 18(b) shows data for the AIE nozzle. The flight and 22% scale model data for the VFE nozzle agree very well from Mach 0.6 to 0.9 and agree fairly well from Mach 1.1 to 1.27. At Mach 0.95, the flight data rises above the model data and then falls below the model data at Mach 1.0.

In this Mach range, a terminal shock moves off the rear of the nacelle and the boattail flow becomes supersonic. Model blockage effects retard the passage of this shock system over the model with increasing Mach number, and the drag rise of the model is delayed until Mach 1.0 or higher.

The same sort of blockage effect is also present in the AIE nozzle data. But in addition, the flight and model performance data for the AIE nozzle do not agree at Mach numbers below 0.9. Since model data in reference 8 has shown that the flow through the auxiliary inlet doors of the nozzle is separated from the doors, the performance of nozzles of this type may be Reynolds number sensitive. Therefore, to be sure of the performance of nozzles which may have regions of separated flow, it may be necessary to test at the full scale Reynolds number.

CONCLUDING REMARKS

A 5.5-inch diameter turbojet engine simulator was designed and fabricated to simulate the inlet mass flow ratios and nozzle pressure ratios for a modern high pressure ratio turbojet engine at transonic and supersonic speeds. The simulator reliably provided the proper values of these parameters for a J85-13 turbojet engine at minimum reheat power setting over a range of Mach numbers from 0.6 to 1.27. It is important to note that the pressure ratio and flow ranges demonstrated in this test are also typical for low by-pass mixed flow turbofan engines at subsonic cruising speeds.

Nozzle performance data obtained with the 0.22-scale model of the F-106B was free from tunnel blockage effects up to and including Mach 0.9 and to a lesser degree at Mach 1.09 and above. Tunnel blockage effects were present at tunnel Mach numbers of 0.95 and 1.00. At Mach

numbers free from tunnel blockage effects, the 0.22-scale VFE nozzle performance data agreed very well with the full-scale nozzle performance data obtained in flight. Model and flight nozzle performance data for the AIE nozzle did not agree below Mach 0.9, indicating the possibility of a Reynolds number effect on the performance of auxiliary inlet nozzles with separated flows.

REFERENCES

1. Fasano, A , Erlandsen, P., and Barrett, D., "The Powered Nacelle as an Experimental Tool," Paper 70-636, June 1970, AIAA, New York, N.Y.

2. Welge, H. R. and Ongarato, J. R., "Powered Engine Simulator Procedures and Experience for the DC-10 Wing Engine at High Subsonic Speeds," Paper 70-590, May 1970, AIAA, New York, N.Y.

3. Groth, H. W., Samanich, N. E., and Blumenthal, P. Z., "Inflight Thrust Measuring System for Underwing Nacelles Installed on a Modified F-106 Aircraft," TM X-2356, 1971, NASA, Cleveland, Ohio.

4. Vanco, M. R., "Performance Data for a Small Low-Specific-Speed Ten Stage Turbine Tested in Argon. TM X-52892, 1970, NASA, Cleveland, Ohio.

5. Flagg, E. E., "Analytical Procedure and Computer Program for Determining the Off-Design Performance of Axial Flow Turbines," CR-710, 1967, NASA, Washington, D.C.

6. Head, V. L., "Flight Investigation of an Underwing Nacelle Installation of Three Variable Flap Ejector Nozzles," Proposed NASA Technical Memorandum.

7. Burley, R. R., "Flight Investigation of Airframe Installation Effects in an Auxiliary Inlet Ejector Nozzle on an Underwing Engine Nacelle," TM X-2396, 1971, NASA, Cleveland, Ohio.

8. Johns, A. L. and Steffen, F. W., "Performance of an Auxiliary Inlet Ejector Nozzle with Fixed Inlet Doors and Triple-Hinge Trailing-Edge Flap." TM X-2034, 1970, NASA, Cleveland, Ohio.

TABLE I. - TURBINE STAGE GEOMETRIES

Stage number	Stator			Rotor		
	Number of blades	Diameter		Number of blades	Diameter	
		Inlet	Exit		Inlet	Exit
1	27	1.600 1.350	1.600 1.350	31	1.600 1.340	1.600 1.250
2	27	1.600 1.240	1.600 1.150	29	1.600 1.140	1.600 1.100
3	26	1.600 1.090	1.600 1.050	27	1.600 1.040	1.600 1.000

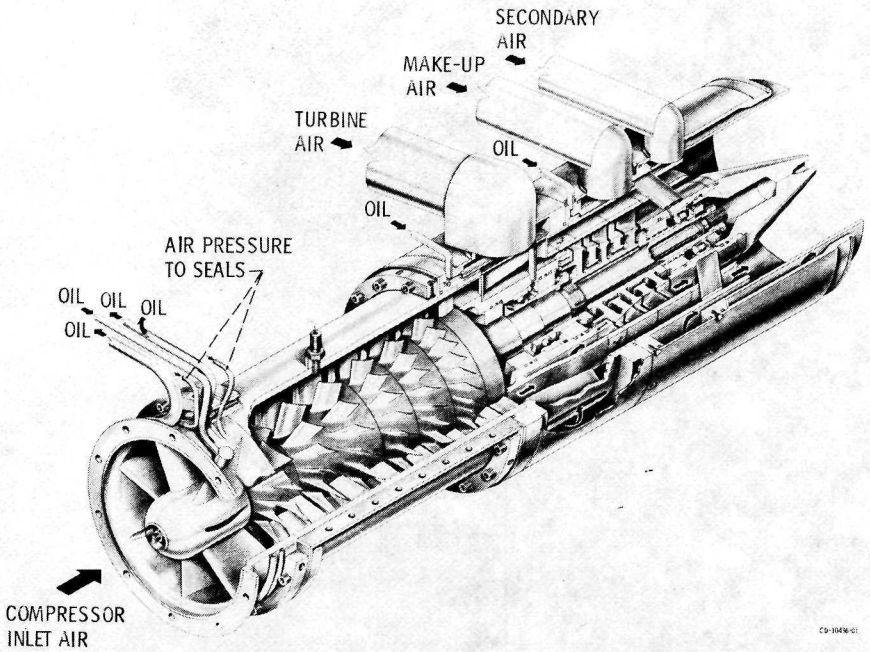

Figure 1. - Isometric view of turbojet engine simulator.

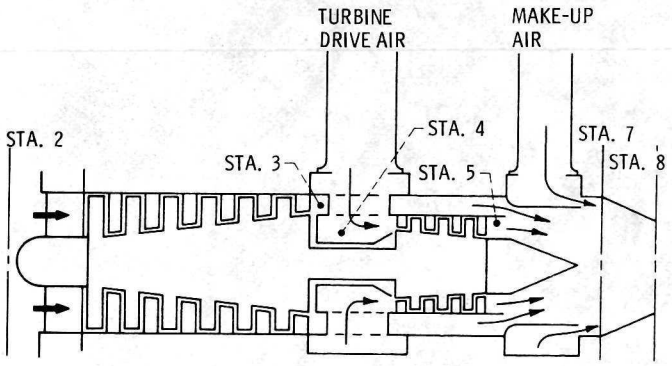

Figure 2. - Schematic view of turbojet engine simulator.

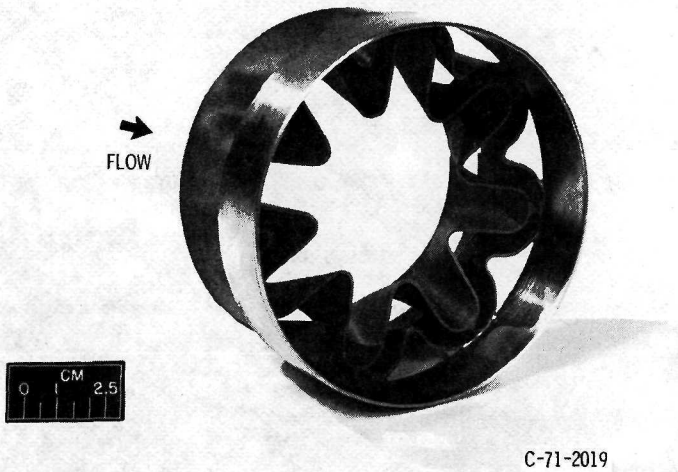

C-71-2019

Figure 3. - Daisey mixer.

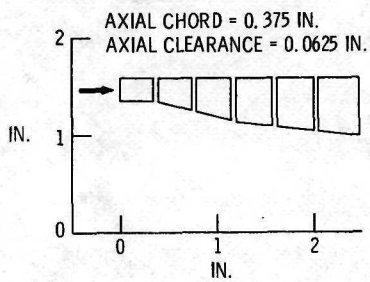

Figure 4. - Turbine flow path.

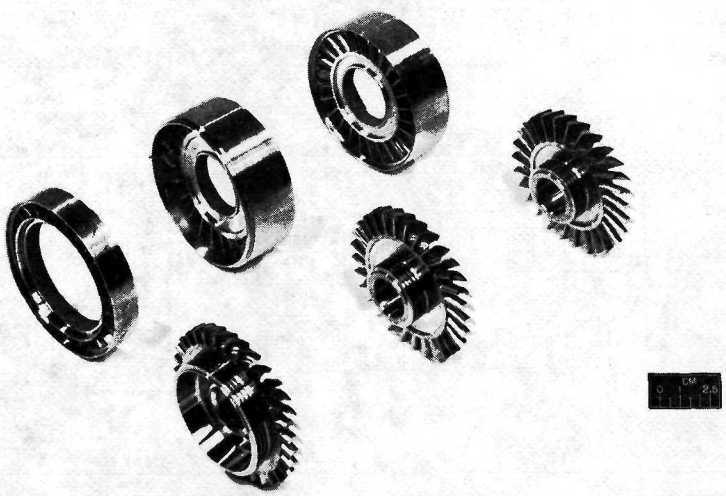

C-71-2018

Figure 5. - Exploded view of turbine for turbojet simulator.

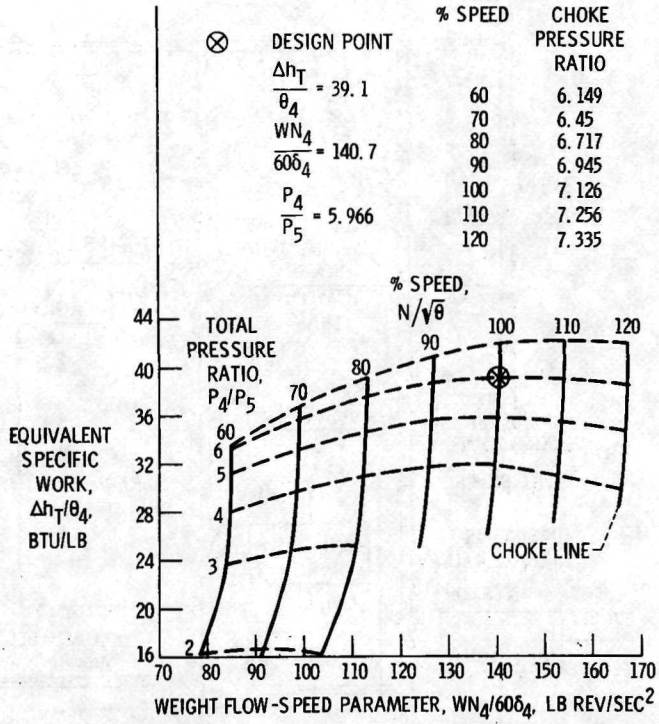

Figure 6. - Analytical turbine map for three stage simulator turbine.

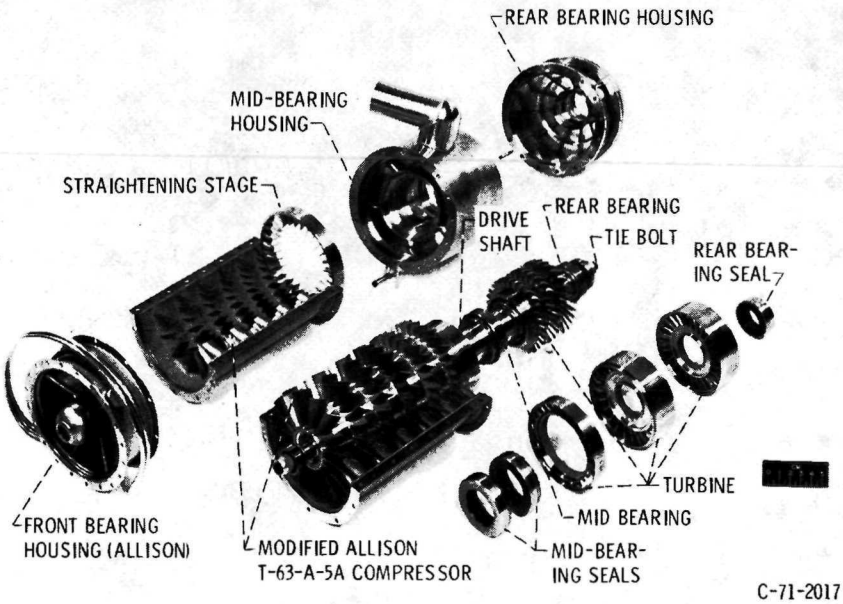

Figure 7. - Exploded view of turbojet simulator.

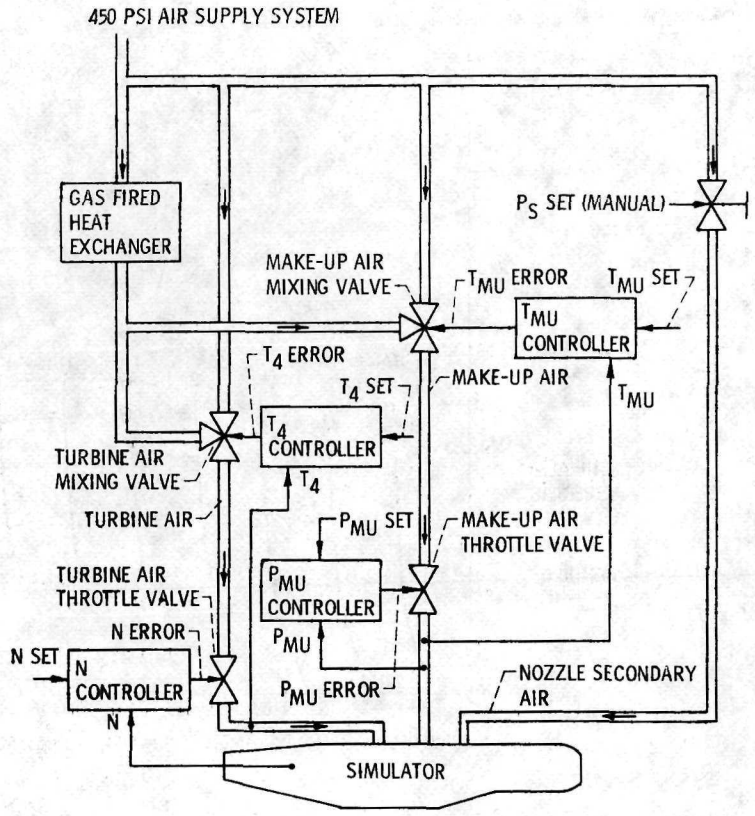

Figure 8. - Simulator air supply and control systems.

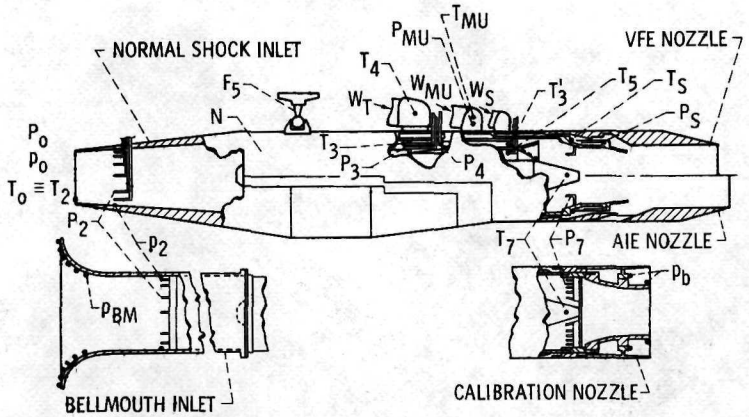

Figure 9. - Research instrumentation.

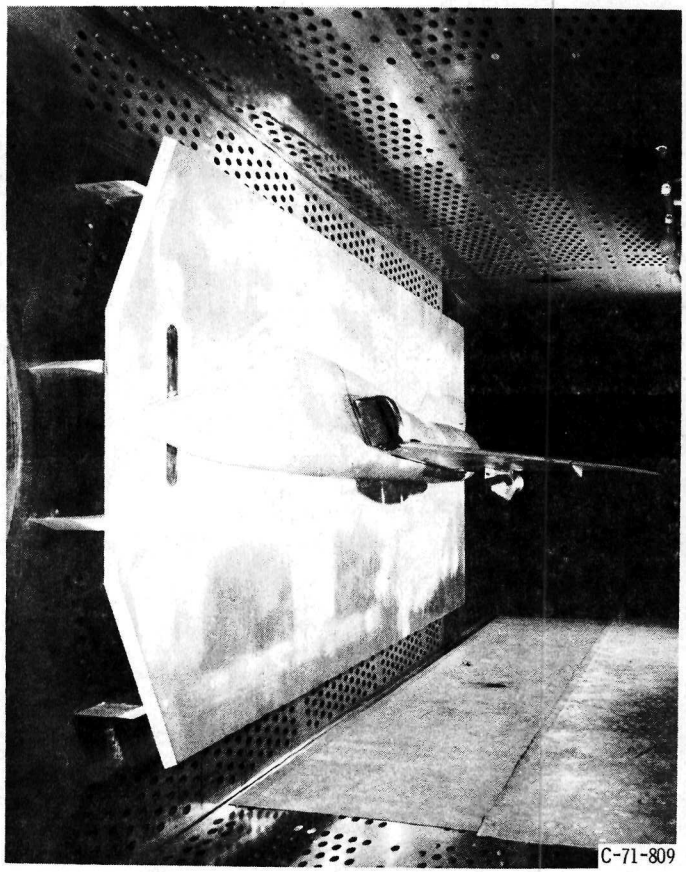

Figure 10. - Installation of .22 scale F-106B model with turbojet simulator in 8x6 Supersonic Wind Tunnel.

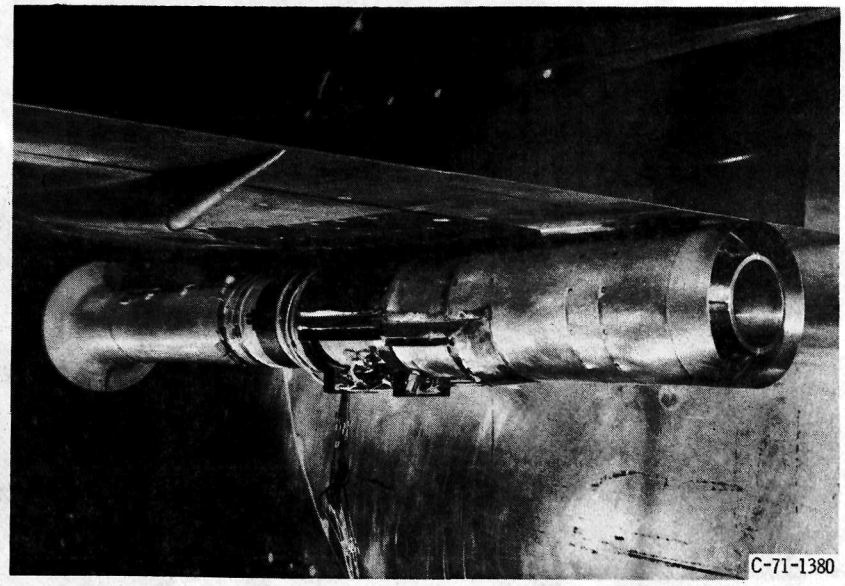

(a) NACELLE WITH CALIBRATION NOZZLE AND BELLMOUTH INLET.

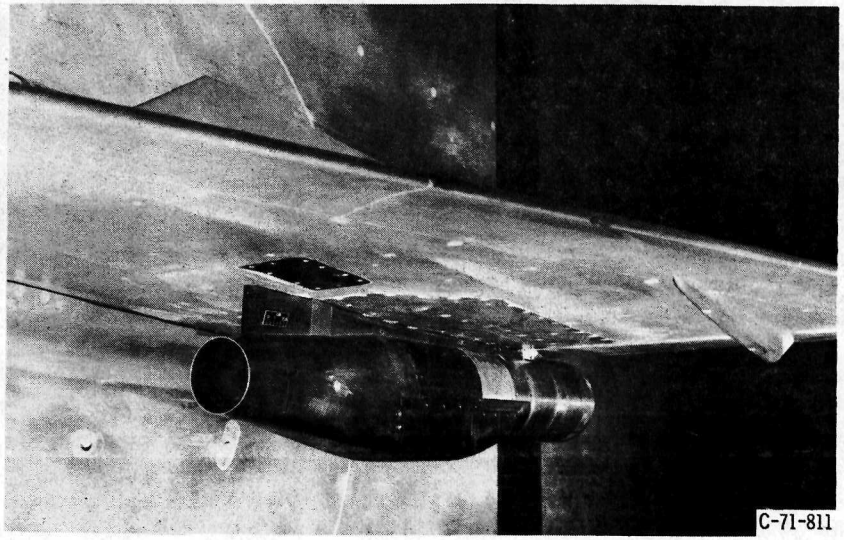

(b) NACELLE WITH CALIBRATION NOZZLE AND NORMAL SHOCK INLET.

Figure 11. - Calibration configurations.

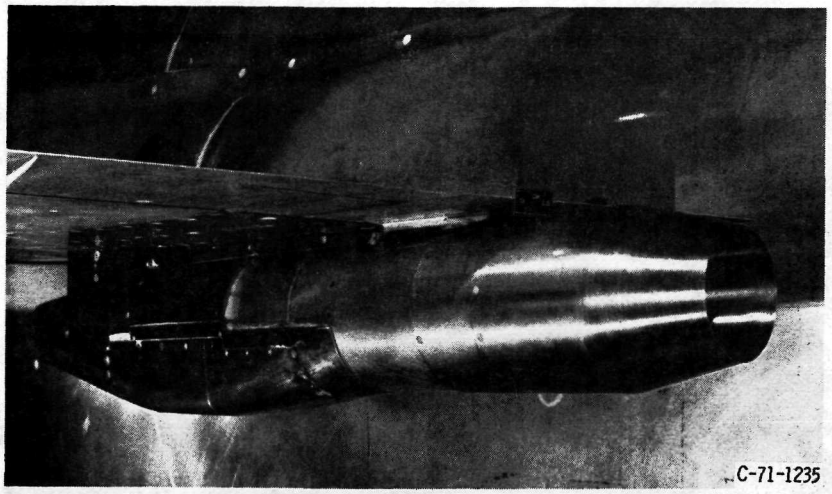

(a) NACELLE WITH VFE NOZZLE AND NORMAL SHOCK INLET.

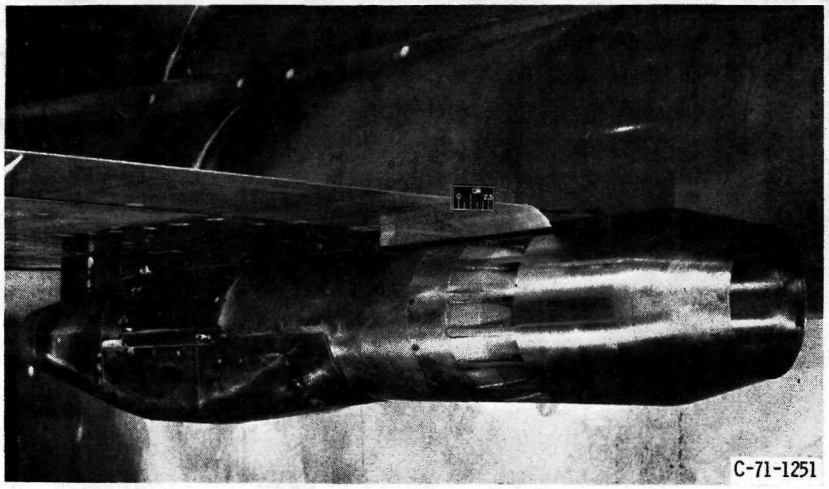

(b) NACELLE WITH AIE NOZZLE AND NORMAL SHOCK INLET.

Figure 12. - Nozzle research configurations.

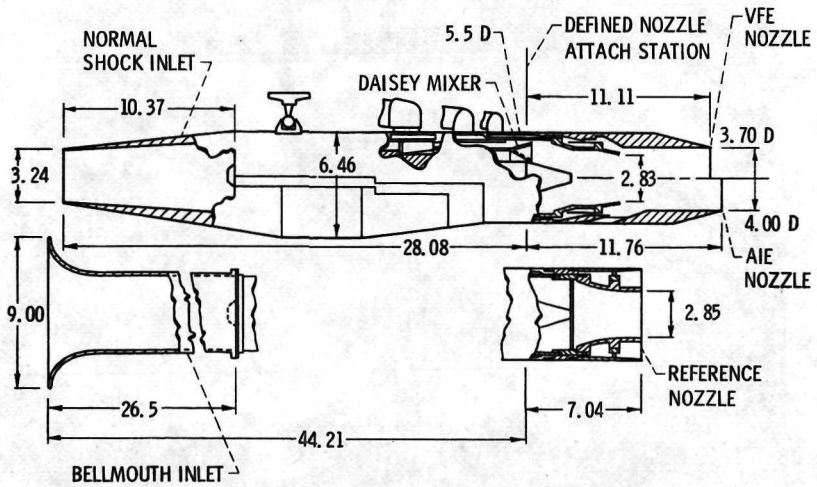

Figure 13. - Nozzle and nacelle dimensions. Dimensions are in inches.

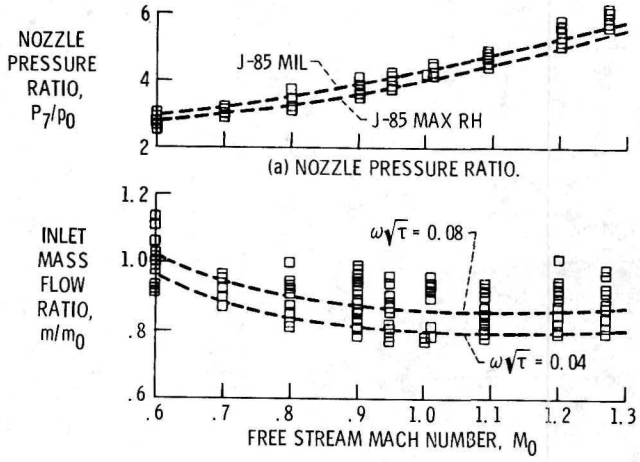

(a) NOZZLE PRESSURE RATIO.

(b) INLET MASS FLOW RATIO.

Figure 14. - Range of nozzle pressure ratios and inlet mass flow ratios achieved during simulation of installed J-85 engine at minimum reheat power setting.

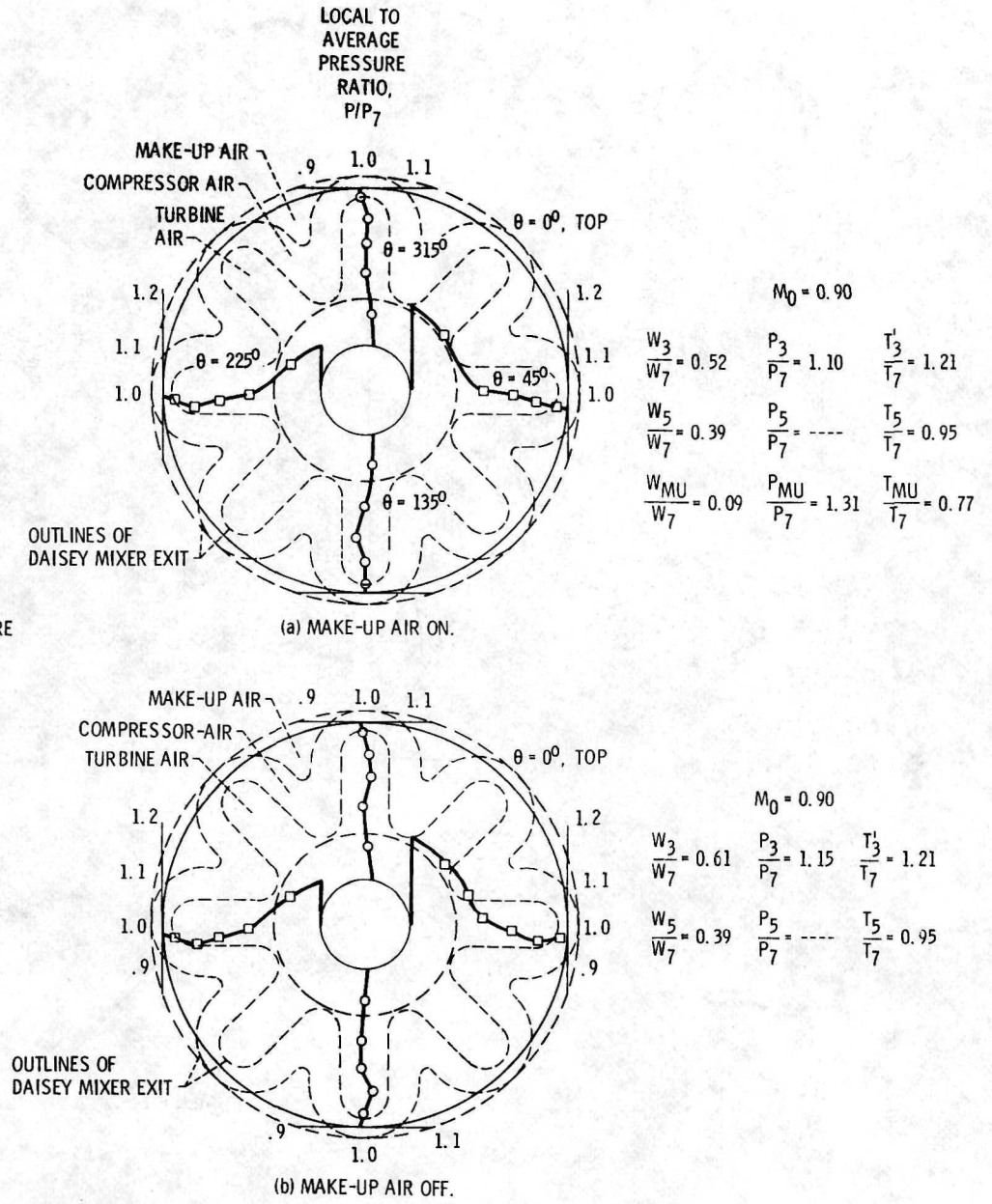

(a) MAKE-UP AIR ON.

(b) MAKE-UP AIR OFF.

Figure 15. - Pressure and temperature profiles at station 7. View looking downstream.

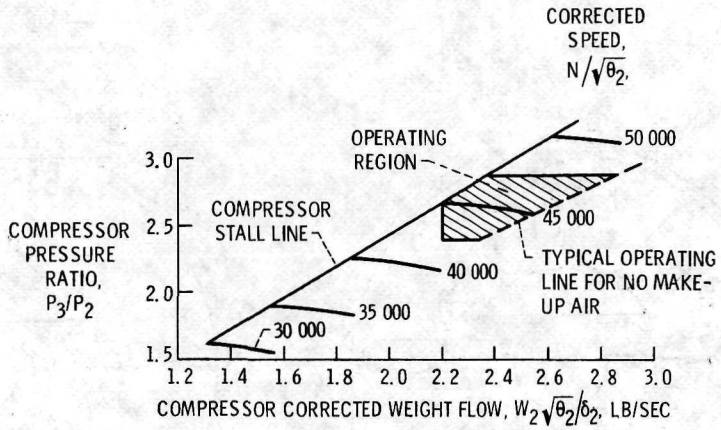

Figure 16. - Allison T-63 axial flow compressor map.

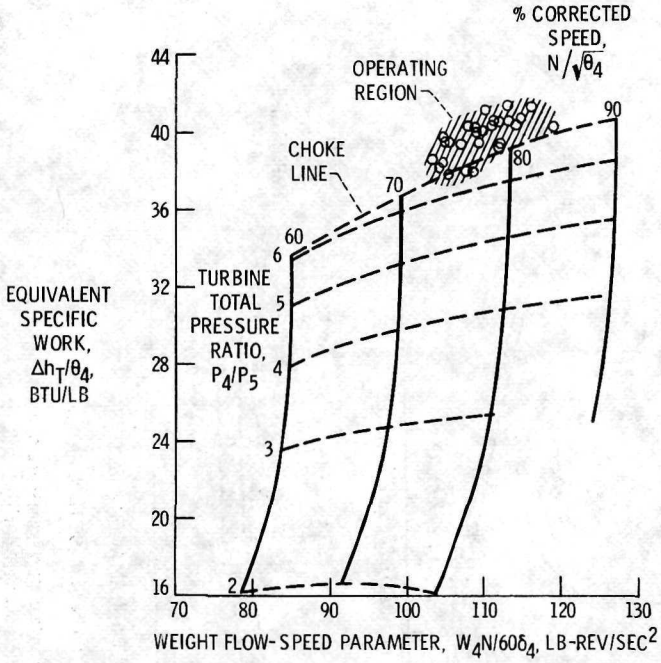

Figure 17. - Operating range of turbine during initial application.

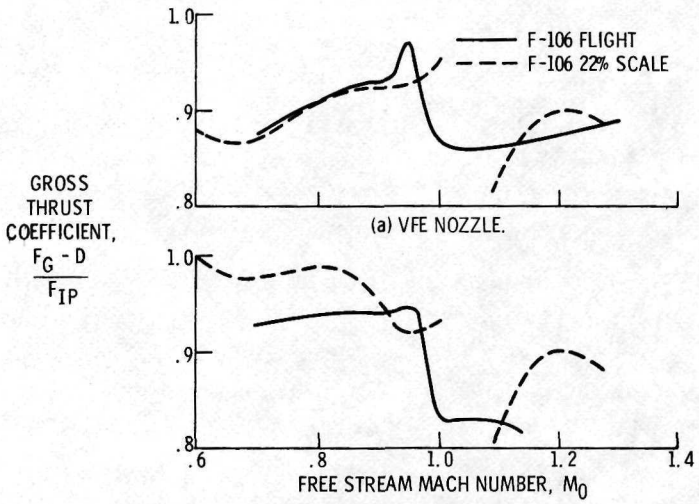

Figure 18. - Installed nozzle performance.